Chapter 2

Multipath Propagation, Characterization and Modeling in GNSS

Marios Smyrnaios, Steffen Schön and Marcos Liso Nicolás

Additional information is available at the end of the chapter

http://dx.doi.org/10.5772/54567

1. Introduction

GNSS signals may arrive at the receiving antenna not only through the direct path, i.e. the line-of-sight (LOS) path, but also on multiple indirect paths, due to different electromagnetic effects as signal reflection or diffraction. These signal components arrive with a certain delay, phase, and amplitude difference relative to the LOS component. We will call these signal components multipath components (MPCs) and the phenomena multipath propagation.

Multipath propagation degrades the positioning accuracy. Moreover, in precise applications, multipath errors dominate the total error budget. Despite the different approaches developed, several aspects of multipath propagation are still not fully understood. The generally unknown number of MPCs and their path geometry, the signal characteristics, the diffraction and reflection effects as well as their changing nature together with a complex antenna and receiver design make multipath mitigation very challenging. Furthermore, the site-dependent characteristics of multipath decorrelate the errors caused by multipath propagation at different antenna locations and thus, differential techniques, like e.g. double differences (DD), cannot mitigate it.

The superposition of the MPCs and the LOS signals yields a compound signal at the receiving antenna. Depending on the relative phase between the MPCs and the LOS signal, constructive or destructive interference appears. As a result, during signal tracking the correlation output between the received signal and the local pseudorandom noise (PRN) code replica generated by the receiver is deformed. Since MPCs arrive generally at the receiving antenna with small extra paths, up to 20 m, relative to the LOS signal, the correlation output is biased and the receiver is not able to discriminate between MPC and the

LOS signals. This correlation output is the fundamental input for the next iteration of the code and phase tracking loops of the receiver as well as for C/N_0 estimation algorithms. As a result, the three GNSS observables code-phase, carrier-phase, and C/N_0 are biased by multipath propagation. In this text, errors in code-phase and carrier-phase observations caused by multipath propagation are referred to as code multipath and carrier-phase multipath, respectively, and in general as multipath errors.

In the observation domain, multipath errors are not constant in time. They show a sinusoidal behavior which can be noticed in carrier-phase residuals from Precise Point Positioning (PPP), double differences (DD) or C/N_0 time series. This behavior is due to the change of the relative phase between the direct and indirect signals as the satellite vehicle moves above the local horizon of the antenna. The magnitude of these oscillations depends on the relative amplitude of the MPC which varies as geometry changes. The C/N_0 observable is the only GNSS observation type in which multipath propagation effects are directly visible without any sophisticated data pre-processing. In contrast, in the phase or code domain, residuals should be analyzed or differences should be formed in order to eliminate all other errors sources. This is one of the main reasons why signal strength measures have attracted much attention in GNSS multipath studies. Since the relative signal amplitude between the LOS and MPC signals plays a key role for the understanding of multipath propagation and also for the magnitude of the multipath error in the GNSS observables, the following contribution focuses on an extended description and proposes an analytical model for modeling GNSS signal amplitudes.

This chapter is structured as follows. A compact overview on different approaches for multipath mitigation or characterization will be presented next. The approaches are categorized into techniques in the observation domain, receiver-internal as well as antenna-related techniques and further methods. Cornerstone methods of each category will be highlighted. In the third section, the multipath phenomenon and its impact on GNSS code, carrier phase and C/N_0 will be summarized. Special emphasize is given to the reflection process including signal polarization. An analytical model for GNSS signal amplitude is proposed. The equations for phase and code errors due to multipath propagation are extended so that the signal amplitude can be analytically calculated for each epoch. Finally, results from a dedicated experiment are shown in order to highlight the key features of multipath propagation.

2. Overview of multipath related studies in GNSS

In the beginning of the 1970s multipath effects on L1 frequency were first studied by [1] and the fundamental relationships between code error due to multipath and the driving parameters were derived. In [2], it was shown that the presence of multipath can be identified by using double differenced phase observations. Since then and during the last 4 decades many researchers have been involved in the characterization and modeling of this propagation phenomenon. A large number of scientific papers have been published on this topic, where different approaches and aspects of the problem have been investi-

http://dx.doi.org/10.5772/54567

gated under certain predefined assumptions. Consequently, the scientific literature on multipath propagation for GNSS positioning can appear very rich for scientists. Despite the large number of different approaches developed, a universal solution of this problem is not achieved until the time of writing. Nevertheless, different promising approaches are under consideration and development.

In almost all textbooks on geodesy or navigation, with very few exceptions (e.g. [3]), multipath propagation is presented in short texts of a couple of pages (e.g. [4, 5, 6]). Most of the time, the phenomenon is explained geometrically, while other physical or electromagnetic properties of the reflected signals are not discussed. The progress in multipath-related studies is documented in various PhD thesis, we cite here exemplarily [7, 8, 9, 10, 11, 12, 13, 14, 15, 16].

A prominent example for the successful reduction of *code multipath* is the smoothing of the code observations by the about two orders of magnitude more precise carrier-phase observations [17]. Some manufacturers apply code smoothing as a default setting in the receiver. Longer smoothing periods give better performance in general [18, 9]. According to [9], the benefits of such an approach can yield a significant reduction of multipath impact given a sufficient large smoothing time constant, e.g. in aviation typically 100 sec are used. However, the variability of the ionospheric conditions may create additional range biases when smoothing. Van Nee in [19] showed that due to the non-zero mean of code-phase multipath, multipath effects cannot be eliminated by simply averaging over longer periods.

One of the most popular methods to characterize and quantify code multipath, are the so-called multipath linear combinations [20]. The original code and carrier-phase observations from dual frequency receivers are combined in such a way, that the code multipath can be isolated. Due to its computational simplicity this approach is often used to assess the overall multipath contamination at continuously operating reference stations (CORS), for example, the IGS network, or to characterize the performance of new receivers or new satellite signals, like e.g., the upcoming Galileo or GPS L5. However, it should be noted that the characterization is only valid if no code smoothing was applied.

Contrary to the code observations, the *multipath error on the carrier phase observations* is restricted in magnitude, since it is smaller than a quarter of the respective wavelength, i.e. about 5 cm maximum for the GPS L1 frequency. However, this is still large compared to the precision that carrier-phase observation could reach. Wanninger and May [21] proposed a method for carrier-phase multipath characterization of GPS reference stations. They analyze the double difference residuals in GPS networks. Consequently, it may sometimes be challenging to assign exactly the multipath signature to a specific site or satellite.

In post-processing, sidereal filtering or sidereal differencing is often applied. Taking advantage of the sidereal repetition of the GPS orbits, observation or coordinate time series of subsequent days can be subtracted in order to reduce the impact of multipath. Genrich and Bock in [22] showed that a reduction of about 80% can be obtained in this way. However, strictly speaking, each GPS satellite has its own, time-varying orbital period differing up to 10 sec with respect to the nominal sidereal period. Different approaches have been proposed to find the correct

individual repeat times cf. [23, 24]. In addition, due to the nodal precession, the satellite ground track deviates over time, so that different reflectors will be illuminated, cf. for exemplary ground track variations [21, 16, 24]. Finally, changing weather conditions like rain or snow will influence the reflection properties of the antenna vicinity, so that the similarity of multipath errors is reduced. All three effects restrict the power of multipath mitigation by sidereal differencing, especially over longer time intervals.

Finally, the analysis of un-differenced carrier-phase residuals from PPP is a useful tool for accessing the impact of multipath effects [25]. For this purpose, the residuals are color-coded and depicted in a sky-plot. The variations of the residuals translate into a sequence of concentric rings in the sky-plot. But, since PPP residuals contain further remaining systematic effects, like e.g., varying tropospheric refraction, averaging strategies may be necessary [26].

Observations of the *signal strength*, like SNR or C/N_0, have attracted much attention in multipath related studies although most of the approaches are found in post-processing applications [27]. Compared to code or carrier-phase observations, the C/N_0 values are usable without sophisticated pre-processing steps and attributed to one satellite-receiver propagation channel, i.e. no double differences are formed. First results of this type of investigation were presented in [28] while newer ones can be found in [29, 27, 10]. The basic idea is that the C/N_0 values follow a nominal curve with respect to the satellite elevation that is mainly determined by the antenna gain pattern. Thus, deviations from this pattern can be easily identified and attributed to reflected and/or diffracted signals. Although, the qualitative analysis is straight-forward, a quantitative analysis of multipath by C/N_0 is still limited. The major restrictions are (i) proprietary algorithms and definitions of the C/N_0 values given by the commercial receivers. Different manufactures use different algorithms for the calculation of this type of observations. (ii) Different receivers (especially older ones) use different quantization levels (e.g. 1 dB-Hz instead of 0.1 dB-Hz) which can be very coarse for certain type of applications. (iii), the gain pattern of the receiving antenna is often unknown. Then empirical methods are proposed to determine the form of the C/N_0 curves [29, 27, 10]. Recently and very encouraging, some antenna manufacturers have published receiver antenna gain patterns for right-hand and left- hand circular polarization [30]. It would be very useful if in future more manufacturers could follow this example. Finally, C/N_0-based observation weighting has been found to be very efficient to reduce the impact of reflection and/or diffraction effects on the observation level [31, 32, 33].

Receiver-internal multipath mitigation/detection techniques incorporate different signal processing strategies for the reduction of this type of errors. The cornerstone approach for this category of approaches is the narrow-correlator technology [34]. It was demonstrated that by reducing the spacing of the early and late correlators from 1 chip to 0.1 chips, a significant reduction of multipath error could be achieved. In this way, MPCs with large extra path delay could be filtered out. Since then, several other approaches were developed, most of them for the mitigation of code multipath and much fewer for phase multipath. The majority of the internal approaches incorporate the use of several early and late correlators with different spacing between them. The correlator outputs are then used for the formation of different multipath mitigation discriminators or for the detection of the deformed slopes of the correlation peak.

One of the most characteristic approaches is the High Resolution Correlator [35], where the code discriminator is formed by two pairs of early-late correlators. Strobe Correlator [36, 37] and Vision Correlator [38] are other receiver internal techniques. A major breakthrough in the receiver internal approaches happened in 1995, when Novatel introduced the Multipath Estimating Delay-Lock Loop (MEDLL) [39, 40]. According to [41], the MEDLL is a maximum likelihood estimation technique pioneered by Van Nee [11] at Delft University of Technology and it improves the C/A-code narrow correlator performance by configuring the residual pseudorange error to a smaller region of secondary path relative delay. Since then, different approaches have been developed incorporating multiple correlators and estimation theory. Despite the evolvement of the receiver internal mitigation approaches, MPCs of relative short extra paths (less that 30 m) still cause errors in all types of GNSS observables. An overview work on receiver internal approaches with very interesting references can be found in [9, 42]. In addition, aspects on multipath propagation and the impact on the receiver's signal processing modules can be found in text books about software-defined GNSS receivers, like [43, 44, 45].

A lot of effort was given on the *antenna design*. In [46], basic aspects of a GNSS antenna are presented. A first approach consists in using antenna elements with a large ground-plane which increases the directivity of the antenna for the upper hemisphere and reduces reflections from below the antenna horizon. However, diffraction at the edges occurs and cause severe problems e.g. [47]. Subsequently, choke ring antennas were developed [48] and are widely used now, especially for reference station applications. Even though they attenuate MPCs coming from negative elevation angles with respect to the antenna horizon, their design cannot mitigate MPCs coming from positive elevation angles. Modern designs use variable choke-ring depths [49]. Assuming a change of polarization of the RHCP GNSS signals upon reflection, a basic principle applied in all GNSS antennas is to increase the sensitivity for RHCP and to simultaneously decrease the sensitivity of LHCP signals. Finally, it should be stated that different attempts to reduce the multipath reflection by applying micro-wave absorbing material are reported in literature, e.g. [50].

Closely-spaced antennas [12, 51] are also developed for the reduction of multipath errors. They form a type of small antenna arrays. Based on a least-squares adjustment, the multipath relative amplitude α, the multipath relative phase ($\Delta\Phi$) as well as azimuth and elevation of the assumed reflector can be estimated [9]. Further developments leads to beam steering and adaptive beam forming antennas or antenna-receiver combination, like e.g., DLR's GALANT receiver [52]. However, this interesting technology seems to be not mature enough to be installed at GNSS reference stations.

In [53] the concept of *station calibration* for multipath mitigation by a parabolic antenna was presented, however the concept is not in operational use, today. Further approaches of station calibration try to randomize the multipath effect by shifting the antenna in a controlled manner using a robot [15, 54, 55]. This method is very successful for in-situ calibration; however the efforts due to the operation of the robot are very large. The validity of the corrections is again restricted by the individual repeat times of the satellite orbits. In [16, 24] a separation of the so-called near- and far-field multipath is proposed, by calibrating the antenna with and

without its mount, like e.g., tripods or special metal adaptations. The difference in the determined phase center variations is attributed to the near-field multipath.

New GNSS signals with different signal structures (e.g. AltBOC) have a better performance against multipath; cf. e.g. [56, 57, 58]. Nevertheless, short delay MPCs will still cause problems in all types of GNSS signal.

In order to get a better understanding of the physical processes involved in the multipath phenomenon, models from *wave propagation* are very useful. First results were given in [59]. More elaborated models are based on ray-tracing tools that use as a fundamental input the physical environment in which the antenna is placed, the receiving antenna position and the transmitting antenna position. Based on these input parameters, all possible signal paths are estimated and the geometric and electromagnetic properties of them are calculated. Ray-tracing tools are widely used for the simulation of wireless networks. In GNSS-related studies they were presented in [8] and [60]. Another ray-tracing approach [14] was used for the characterization and modeling of P-code multipath in different environments. Based on digital terrain models, more complex scenarios like urban canyons are analyzed, cf. [61]. Besides deterministic channel models, stochastic modeling is applied in complex scenarios, like e.g., DLR's land mobile and aeronautic channel model [62] and subsequent work.

In recent years, the concept of GNSS reflectometry and scatterometry has strongly evolved, cf. e.g., [63, 64, 65, 66, 67, 68, 69]. Here multipath propagation is not considered as bias but as basic information. In the context of GNSS-R, much progress has been made, especially in the mathematical and physical modeling of the wave propagation. Hence, these publications can be a valuable source for mitigating multipath in positioning.

3. Multipath characterization

3.1. Basic considerations

After reaching the receiving antenna, the GNSS signals are down-converted from radio-frequency (RF) to an intermediate frequency (IF) by the RF front-end of the receiver. Afterwards, the signal is digitized, down-converted to baseband and correlated with locally-generated replicas of the PRN codes. Then, the result of the correlation is accumulated for a certain time interval. In a typical GNSS receiver architecture, three replicas for each PRN code are generated, the so-called prompt, early and late replicas. The resulting correlation outputs of the prompt replica of the PRN code in the presence of a number of k MPCs are written as in [34, 17]:

$$I_P = AD(\tau)R(\tau)\cos(\theta_{dir}) + A\sum_{k=1}^{n} \alpha_k D(\tau)R(\tau - \Delta\tau_k)\cos(\theta_{dir} + \Delta\Phi_k), \quad (1)$$

$$Q_P = AD(\tau)R(\tau)\sin(\theta_{dir}) + A\sum_{k=1}^{n} \alpha_k D(\tau)R(\tau - \Delta\tau_k)\sin(\theta_{dir} + \Delta\Phi_k), \quad (2)$$

http://dx.doi.org/10.5772/54567

where A is the amplitude of the direct signal, D is the navigation bit, R is the correlation function, τ is the code tracking error and θ_{dir} is the phase of the LOS component. The multipath components are characterized by the relative amplitude of the k-th MPC α_k the relative delay $\Delta\tau_k$ and the relative phase $\Delta\Phi_k$ with respect to the LOS signal. Equations for the early and late replicas of the signal can be written in a similar way, although in these cases the chip spacing should also be considered.

Based on the correlation outputs (I_P and Q_P) of the prompt correlator, a GNSS receiver is able to calculate the amplitude (A_c) and phase (θ_c) of the compound signal (see Figure 1). However, the characteristics of the direct and the MPC signals cannot be estimated since the geometry is not known and the receiver cannot discriminate between them, especially in the case of short delay MPCs. In Figure 1, a vectorial representation for the case of the direct component and one multipath component is presented. The direct signal component is characterized by a certain phase (θ_d) and amplitude (A_d), while the MPC is characterized by a relative phase ($\Delta\Phi$) and a relative amplitude (α) with respect to the direct component. It should be mentioned that due to the motion of the satellite and maybe of the receiving antenna, none of the above parameters is constant in time. Directly from this vector diagram, an expression for the phase error and the amplitude of the compound signal can be derived as in [2, 3]:

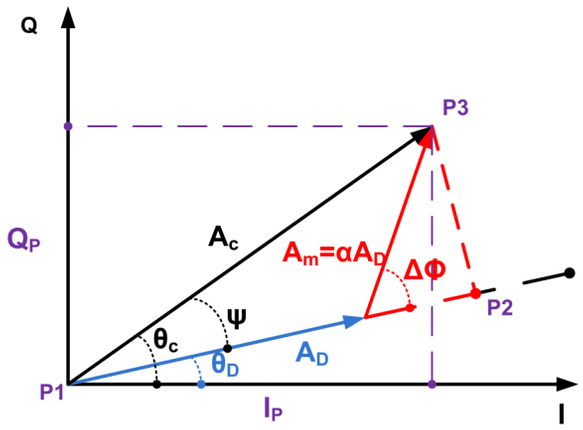

Figure 1. Phase error of PLL due to one multipath component

Assuming a perfect tracking (i.e. R=1) and the relationship $A_m = \alpha A_d$, the phase error (ψ) can be expressed as a function of α and $\Delta\Phi$:

$$\tan\psi = \frac{A_m \sin\Delta\Phi}{A_d + A_m \cos\Delta\Phi} => \psi = \arctan\left(\frac{\alpha \sin\Delta\Phi}{1 + \alpha\cos\Delta\Phi}\right) \quad (3)$$

The compound signal amplitude can be derived as a function of α, $\Delta\Phi$ and A_d from the orthogonal triangle (P1 P2 P3):

$$A_c^2 = \left(A_d + A_m \cos\Delta\Phi\right)^2 + A_m^2 \sin^2\Delta\Phi$$

By using trigonometric identities, the expression for the compound signal amplitude is rearranged as:

$$A_c^2 = A_d^2 + 2\alpha A_d^2 \cos\Delta\Phi + \alpha^2 A_d^2. \tag{4}$$

An equation for pseudo-range error (ϱ) is given in [13]:

$$\varrho = \frac{\alpha\delta\cos\Delta\Phi}{1 + \alpha\cos\Delta\Phi}, \tag{5}$$

with δ being the extra path length of the MPC expressed in meters.

From equations (3), (4) and (5) the 90° phase shift between errors in code, amplitude domains and phase domain can be noticed. When ΔΦ=0°/180° and ψ=0, then ϱ, A_c are maximum/minimum respectively, while when ΔΦ=90°, then ψ is maximum and ϱ=0. Furthermore, for a number of k multipath components, equations (3), (4) and (5) can be written as:

$$\Psi = \arctan\left(\frac{\sum_{k=1}^{n} \alpha_k \sin\Delta\Phi_k}{1 + \sum_{k=1}^{n} \alpha_k \cos\Delta\Phi_k}\right), \tag{6}$$

$$A_c = A_d\sqrt{\left(1 + \sum_{k=1}^{n} \alpha_k \cos\Delta\Phi_k\right)^2 + \left(\sum_{k=1}^{n} \alpha_k \sin\Delta\Phi_k\right)^2}, \tag{7}$$

$$\varrho = \frac{\sum_{k=1}^{n} \alpha_k \delta_k \cos\Delta\Phi_k}{1 + \sum_{k=1}^{n} \alpha_k \cos\Delta\Phi_k}. \tag{8}$$

The relative phase of each multipath component can be expressed as a function of the extra path length (δ) and the wavelength of the carrier signal: $\Delta\Phi = 2\pi\delta/\lambda$, where δ is expressed in meters. Moreover, δ is a function of station height and reflection angle, which in turns depends on the satellite elevation and the orientation of the reflector in space. In the special case of ground multipath, which we will investigate in the following parts of this chapter, the extra path delay is a function of the station height (h) and the satellite elevation (el):

$$\delta = 2h\sin(el). \tag{9}$$

In conclusion, it can be stated that some of the introduced equations can be calculated based on the geometry of the scenario. The signal amplitudes for both LOS and MPC are not directly accessible. However, this information or at least the relative amplitude is a crucial part of all introduced formulas. Therefore, in the following an analytical model of the relative amplitude α is developed.

http://dx.doi.org/10.5772/54567

3.2. Polarization state of the GNSS Signals

In order to understand the amplitude relation between the LOS and the MPCs, in a first step, the polarization state of a signal is introduced and linked to the right-hand circular polarization (RHCP) of the GNSS signal. According to [70], there are many ways to represent the polarization state of a signal or of an antenna. Some are graphic in nature (e.g. Poincaré sphere) and can be easily visualized, while others can be more appropriate for specific applications, like e.g., investigation of antenna wave interaction (e.g. Stokes parameters and/or complex vector representation).

In the case of a circularly polarized (CP) planar wave, the electric field vector is propagating in a helical way (see Figure 2a), where the projection of the tip of this vector forms a circle in a fixed plane normal to the direction of propagation (z). The clockwise or counter clockwise sense of rotation of the electric field vector looking towards the direction of propagation defines whether the signal is left or right-hand circularly polarized, respectively. At each instant in time, the electric field vector is a combination of two components (see Figure 2 b, c):

$$\vec{E}(t) = E_1 \cos(\omega t)\vec{x} + E_2 \cos(\omega t + \zeta)\vec{y}, \tag{10}$$

where E_1 and E_2 are the amplitudes of the instantaneous electric field [V/m] in x and y directions, respectively, ω is the angular frequency in [radians/sec] and ζ is the relative phase shift [radians] by which the y component leads the x component.

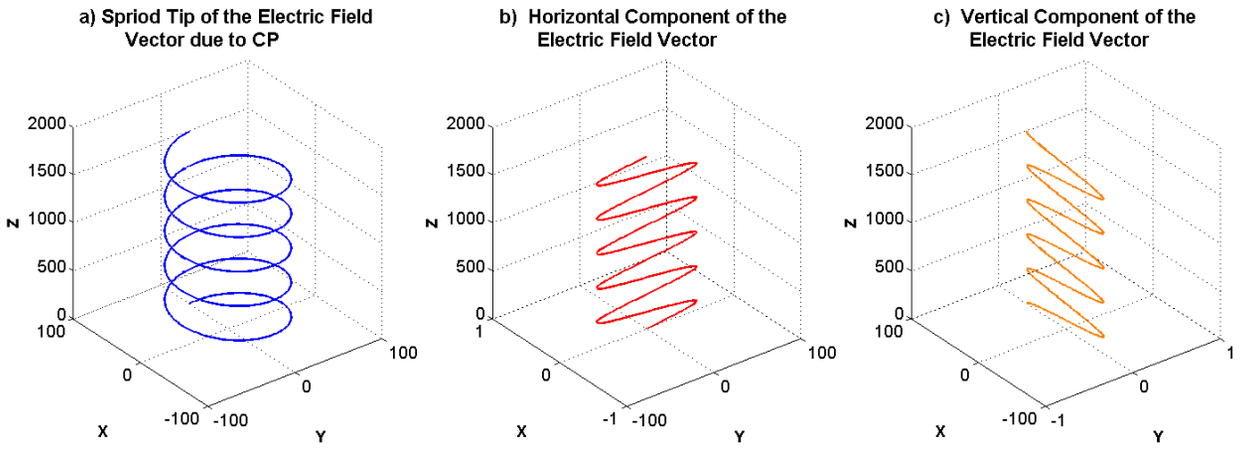

Figure 2. The combination of the two electric field components, in horizontal and vertical direction, results in the CP electric field vector, propagating in z direction in a spiroidal way

Each of the two components represents a linearly polarized wave. When $E_2 = 0$, the wave has a linearly polarization along the x-axis and when $E_1 = 0$, the wave is linearly polarized along the y-axis. Furthermore, if $E_1 = E_2$ and ζ=0°, then the wave is linearly polarized with a 45° tilt. In general, it can be stated that the polarization of a signal can be completely described by the

relative amplitudes and phase of these two components. For circular polarization, there are two requirements on the linear components [71]: i) time quadrature, i.e. $\zeta = \pi/2$ for LH or $\zeta = -\pi/2$ for RH polarization, and ii) equal amplitude, i.e. ($E_1 = E_2$).

Another decomposition of the electric field vector yields orthogonal circular polarization states (LHCP and RHCP). Furthermore, the electric field phasor expressed in terms of CP phasors can be written as [70]:

$$\vec{E}(t) = \vec{E}_L(t) + \vec{E}_R(t) = \frac{\left[\left(E_{L0} + E_{R0}\, e^{j\zeta}\right)\vec{x} + j\left(E_{L0} - E_{R0}\, e^{j\zeta}\right)\vec{y}\right]}{\sqrt{2}}, \tag{11}$$

where $E_{L\,0}$ and E_{R0} are the amplitude of the two orthogonal components.

Finally, the Jones vector is a further way for the representation of signal polarization. According to [72], the Jones vector can be used only for completely polarized signals, e.g. GNSS signals. Equation (10) can be rewritten in complex vector notation as:

$$\vec{E}(t) = \left(|E_1| e^{j\zeta_x}\vec{x} + |E_2| e^{j\zeta_y}\vec{y}\right)e^{j\omega t}, \tag{12}$$

where the relative phase shift between the two electric field components is $\zeta = \zeta_x - \zeta_y$ (see Figure 3). According to [72], this can be further factorized as:

$$\vec{e} = A\vec{x} + Be^{j\zeta}\vec{y}, \tag{13}$$

which is the so-called Jones vector ($\vec{e}$) and the coefficients A and B are:

$$A = \frac{|E_1|}{\sqrt{|E_1|^2 + |E_2|^2}}, \quad B = \frac{|E_2|}{\sqrt{|E_1|^2 + |E_2|^2}},$$

where $A^2+B^2=1$ and the E_{eff} represents the strength of an effective linearly polarized wave that would give the same intensity that is described by eq. (10) [72].

$$E_{eff} = \sqrt{|E_1|^2 + |E_2|^2}\, e^{j\zeta_x}.$$

Eq. (13) can be written in a column vector form as:

$$\vec{e} = \begin{bmatrix} A \\ Be^{j\zeta} \end{bmatrix}. \tag{14}$$

http://dx.doi.org/10.5772/54567

Eq. (14) completely describes the polarization state of GNSS signals since information of the amplitude of both electric field components as well as their relative phase can be extracted. Particular cases for the Jones vector can be seen in Table 1:

Polarization State	
Linearly polarized in x direction	$\begin{bmatrix}1\\0\end{bmatrix}$
Linearly polarized in y direction	$\begin{bmatrix}0\\1\end{bmatrix}$
Right-hand circularly polarized (RHCP)	$\frac{1}{\sqrt{2}}\begin{bmatrix}1\\-j\end{bmatrix}$, with $\zeta = -90°$
Left-hand circularly polarized (LHCP)	$\frac{1}{\sqrt{2}}\begin{bmatrix}1\\j\end{bmatrix}$, with $\zeta = 90°$

Table 1. Jones vector representation for the polarization state of characteristic cases.

3.3. Reflection process

In multipath propagation, one or multiple reflections as well as diffraction of the transmitted signal may occur. In the following, we focus on the description of the reflection process. In the case of reflection of the incident field, the reflection coefficients will indicate how much the reflected field will be attenuated and how the polarization state of the incident field will be deformed. The reflection coefficients used in this investigation are as in [7]:

$$R_{\perp}(\theta_{ref}) = \frac{\cos\theta_{ref} - \sqrt{Y - \sin^2\theta_{ref}}}{\cos\theta_{ref} + \sqrt{Y - \sin^2\theta_{ref}}}, \tag{15}$$

$$R_{\parallel}(\theta_{ref}) = \frac{Y\cos\theta_{ref} - \sqrt{Y - \sin^2\theta_{ref}}}{Y\cos\theta_{ref} + \sqrt{Y - \sin^2\theta_{ref}}}, \tag{16}$$

With

$$Y = \varepsilon - i*60*\lambda*\sigma, \tag{17}$$

where θ_{ref} is the reflection angle and λ is the carrier wavelength. The relative permittivity (ε) and conductivity (σ) depend on the material properties of the reflector. Typical values for the material properties for GNSS frequencies can be found in [7]. The exemplary material properties used in this text can be seen in Table 2.

Reflector Material	Relative Permittivity (ε)	Conductivity (σ) [S/m]
Concrete	3	$2*10^{-5}$
Sea Water	20	4
Wet Ground	30	$2*10^{-1}$

Table 2. Material properties of the exemplary reflectors used in this investigation

The reflection coefficients can also be expressed as circular components of the two orthogonal polarizations (R_{co}, R_{cross}):

$$R_{co} = \frac{R_{\perp}(\theta_{ref}) + R_{\parallel}(\theta_{ref})}{2}, \tag{18}$$

$$R_{cross} = \frac{R_{\perp}(\theta_{ref}) - R_{\parallel}(\theta_{ref})}{2}. \tag{19}$$

For the RHCP satellite signals, R_{co} can be associated with the RHCP component, while R_{cross} represents the orthogonal LHCP component.

In Figure 3a), the circular reflection coefficients are plotted for the L1 carrier. The co-polarized components are plotted with solid lines and the cross-polarized with dashed. The material properties of the exemplary materials (see Table 2) were used for the calculation of the reflection coefficients. The reflection coefficients for a concrete reflector are plotted in black, for a sea water reflector in blue, and for a wet ground reflector in red. They indicate how the electrical field components of the incident field will be changed upon reflection, in terms of magnitude and relative phase.

Looking at reflection coefficients for the different reflection angles in Figure 3a) and for a concrete reflector, it can be seen that when the reflection angle approaches 0°, then the cross-polarized components (LHCP component) tends to 0 and the co-polarized components (RHCP component) is 1, i.e. no loss. When the reflection angle is between 0° and 30°, both components exist but still the co-polarized one is larger in magnitude and the reflected signal is right-hand elliptically polarized (RHEP), with the eccentricity of the polarization ellipse getting bigger. At around 30°, the magnitude of the reflection coefficients is equal. In geodetic literature, this angle is referred to as the Brewster angle [7, 9] for a concrete reflector, although this definition deviates from the common use of the Brewster angle in electromagnetic theory. For these material properties (concrete) and for reflection angle of 30°, the reflected signal is linear polarized. When the reflection angle is between 30° and 90°, the cross polarized component has a higher magnitude and this results in a change of the initial polarization from RH to LH. The eccentricity of the ellipse is then getting smaller as the reflection angle increases. When the reflection angle approaches 90°, the reflected signal is LHCP since the co-polarized components is zero. When the material properties change, then the changes on the reflected field are different. For example, the angle for which the magnitude of the circular reflection coefficients is the same, may vary significantly for different reflectors. Furthermore, small

http://dx.doi.org/10.5772/54567

magnitude changes between the two different frequencies (L1 and L2) may occur. These differences may also vary between different reflectors.

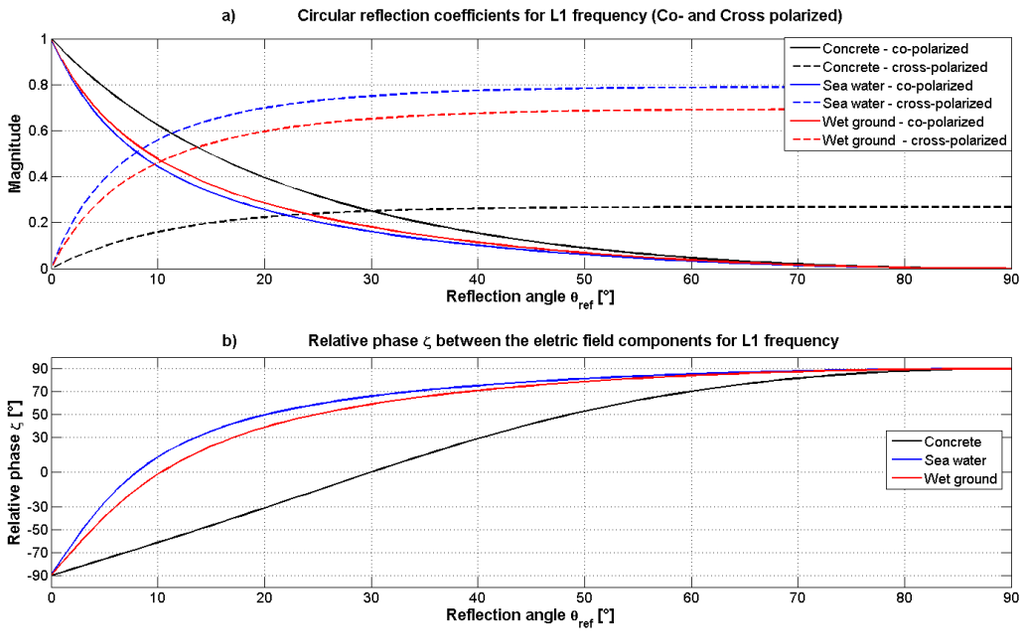

Figure 3. Co- and cross-polarized circular reflection coefficients for L1 (a); and relative phase change between the electric field components due to reflection process for L1 (b). For the exemplary material properties of concrete, sea water and wet ground.

In Figure 3b), the relative phase (ζ) between the field components is illustrated for L1 for the three exemplary material properties. The relative phase between the two components is plotted for all possible reflection angles of the incident field. Without reflection (reflection angle = 0°), the relative phase (ζ) is -90°, which is the relative phase shift for RHCP signals. As the reflection angle increases, ζ is getting smaller and smaller. When the reflection angle is equal to the Brewster angle (for this particular reflector), then ζ=0°, which yields linear polarization. Finally, for reflection angles larger that the Brewster angle, ζ has an opposite sign which indicates that the reflected signal has changed polarization.

3.4. Signal amplitude modeling

According to [73, 74], the signal after the receiving antenna can be written as:

$$S_R = \vec{e}_{rec}^{H} H \vec{e}_{tran} S_T \quad , \tag{20}$$

where S_R is the received signal, $\vec{e}_{rec}^{H}$ is the Hermitian conjugate of the Jones vector of the receiving antenna, and $\vec{e}_{tran}$, is the Jones vector of the transmitting antenna. They are derived

from the antenna gain patterns (for both RH and LH circular polarizations) and thus depend on of the angle of arrival of the signals to the antenna:

$$\vec{e}_{rec_{(el)}} = \frac{1}{\sqrt{2}}\begin{bmatrix} E_{\theta(el)} \\ -jE_{\varphi(el)} \end{bmatrix} = \frac{1}{\sqrt{2}}\begin{bmatrix} \left(E_{rec_{RHCP(el)}} + E_{rec_{LHCP(el)}}\right) \\ -j\left(E_{rec_{RHCP(el)}} - E_{rec_{LHCP(el)}}\right) \end{bmatrix}, \tag{21}$$

More information on the RHCP gain pattern of the satellite antennas can be found in [75]. The signal ellipticity should not be worst that 1.2 dB for L1 and 3.2 dB for L2, [76].

$$\vec{e}_{tran_{(el)}} = \frac{1}{\sqrt{2}}\begin{bmatrix} E_{\theta(el)} \\ -jE_{\varphi(el)} \end{bmatrix} = \frac{1}{\sqrt{2}}\begin{bmatrix} \left(E_{tran_{RHCP(el)}} + E_{tran_{LHCP(el)}}\right) \\ -j\left(E_{tran_{RHCP(el)}} - E_{tran_{LHCP(el)}}\right) \end{bmatrix}. \tag{22}$$

The matrix H is defined for the MPC components as:

$$\begin{aligned} H_{MPC} &= A_{MPC} e^{-j\beta} H_{ref}, \quad \text{a} \\ H_{LOS} &= A_{LOS} e^{-j\alpha}, \quad \text{b} \end{aligned} \tag{23}$$

and for the LOS components as (23b)

where A_{LOS} and A_{MPC} account for the free-space loss attenuation, which for this investigation may be considered equal. $e^{-j\beta}$ and $e^{-j\alpha}$ introduce the phase changes for the LOS and MPC components respectively caused by the free-space propagation. Finally H_{ref} is the channel polarization matrix for one single reflection:

$$H_{ref} = \begin{bmatrix} \cos\Psi_{rec} & \sin\Psi_{rec} \\ -\sin\Psi_{rec} & \cos\Psi_{rec} \end{bmatrix} * \begin{bmatrix} R_{\perp}(\theta_{ref}) & 0 \\ 0 & R_{\parallel}(\theta_{ref}) \end{bmatrix} * \begin{bmatrix} \cos\Psi_{tran} & \sin\Psi_{tran} \\ -\sin\Psi_{tran} & \cos\Psi_{tran} \end{bmatrix}, \tag{24}$$

where Ψ_{rec} and Ψ_{tran} are the rotation angles between the normal of the incident plane and E_θ component of the electric field vector (see Figure 4), $R_\perp$ and $R_\parallel$ are given by eq. (18) and (19).

This expression is divided into three subsequent matrix multiplications. First, the selected base of the **E** field of the transmitting signal has to be aligned with the coordinate system of the so-called incident plane. This plane is defined by the position of the transmitter, the receiver and the reflection point. Next, the signal attenuation and the polarization change are computed taking the electromagnetic properties of the reflecting material into account (e.g. eq. (15) and (16)). Finally, the resulting **E** vector is rotated into the coordinate system associated with the receiving antenna. In this way, both the variation of the orientation of the antennas and the impact of the reflection on the polarization state are taken into account. The geometric situation is depicted in Figure 4.

http://dx.doi.org/10.5772/54567

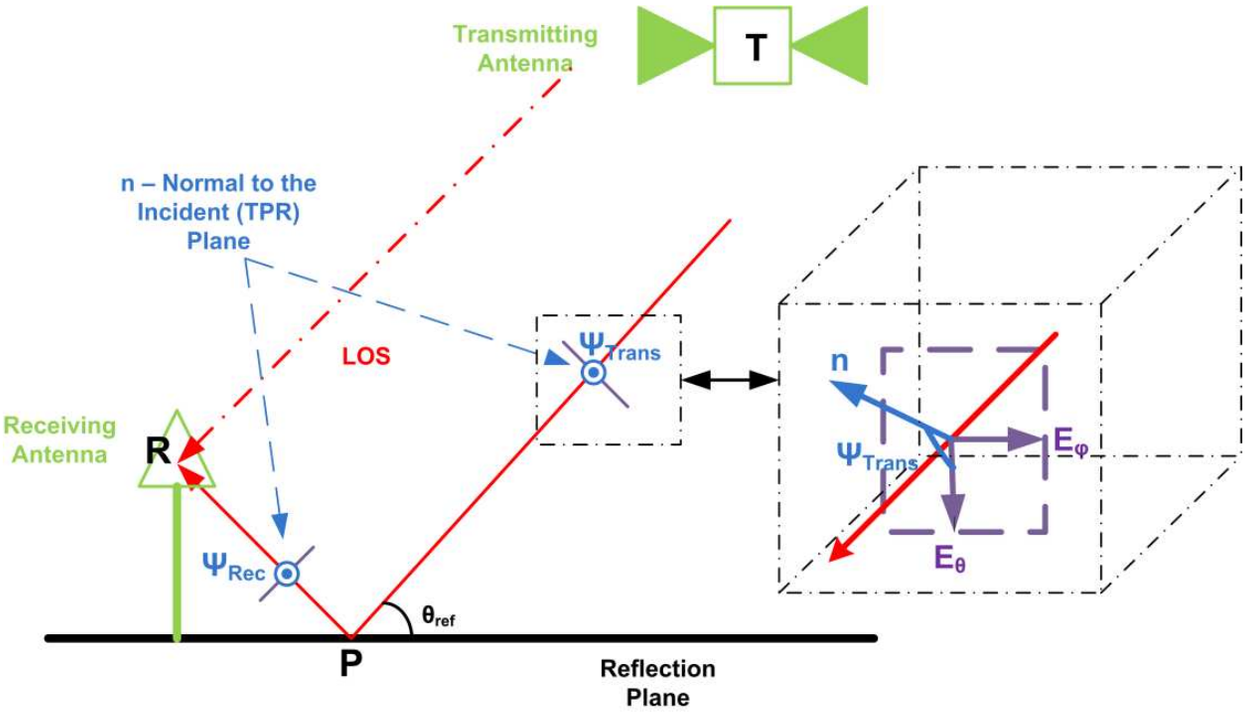

Figure 4. Reflection geometry of ground MPC. The electric field components are expressed in spherical coordinates.

The signal amplitudes for the ground-reflected MPC and for the LOS component are calculated as the absolute values of eq. (25) and (26), where the transmitted signal S_T in this investigation is considered equal to 1. Practically speaking, S_{LOS} reflects the antenna gain pattern value for each specific angle of arrival of the LOS component.

$$S_{MPC} = \vec{e}^{H}_{rec(el+90°)} H_{MPC} \vec{e}_{tran_{(el)}} S_T \,, \quad (25) \tag{25}$$

$$S_{LOS} = \vec{e}^{H}_{rec(el)} H_{LOS} \vec{e}_{tran_{(el)}} S_T \,, \quad (26) \tag{26}$$

yielding the final formulas for the phase error, for the code error and for the compound signal amplitude (for the case of one ground MPC):

$$\psi = \arctan\left(\frac{\left(\frac{|S_{MPC}|}{|S_{LOS}|}\right)\sin(\Delta\Phi)}{1 + \left(\frac{|S_{MPC}|}{|S_{LOS}|}\right)\cos(\Delta\Phi)} \right), \tag{27}$$

$$\varrho = \frac{\left(\frac{|S_{MPC}|}{|S_{LOS}|}\right)\delta\cos(\Delta\Phi)}{1 + \left(\frac{|S_{MPC}|}{|S_{LOS}|}\right)\cos(\Delta\Phi)} \,, \tag{28}$$

$$A_c = |S_{LOS}| \cdot \sqrt{\left(1 + 2\left(\frac{|S_{MPC}|}{|S_{LOS}|}\right)\cos(\Delta\Phi) + \left(\frac{|S_{MPC}|}{|S_{LOS}|}\right)^2\right)}. \tag{29}$$

When multiple multipath components are received, the above equations can be rewritten in a similar way as:

$$\Psi = \arctan\left(\frac{\sum_{k=1}^{n}\left(\frac{|S_{MPC_k}|}{|S_{LOS}|}\right)\sin(\Delta\Phi_k)}{1 + \sum_{k=1}^{n}\left(\frac{|S_{MPC_k}|}{|S_{LOS}|}\right)\cos(\Delta\Phi_k)}\right), \tag{30}$$

$$\varrho = \frac{\sum_{k=1}^{n}\left(\frac{|S_{MPC_k}|}{|S_{LOS}|}\right)\zeta_k\cos(\Delta\Phi_k)}{1 + \sum_{k=1}^{n}\left(\frac{|S_{MPC_k}|}{|S_{LOS}|}\right)\cos(\Delta\Phi_k)}, \tag{31}$$

$$A_c = |S_{LOS}| \cdot \sqrt{\left(1 + \sum_{k=1}^{n}\left(\frac{|S_{MPC_k}|}{|S_{LOS}|}\right)\cos(\Delta\Phi_k)\right)^2 + \left(\sum_{k=1}^{n}\left(\frac{|S_{MPC_k}|}{|S_{LOS}|}\right)\sin(\Delta\Phi_k)\right)^2}. \tag{32}$$

In a similar sense, eq. (1) and (2) can be also rewritten in order to model analytically the relative amplitude factor α which is present also in these equations.

4. Example

4.1. Measurement set up

In order to illustrate the above derived formulas, various experiments were carried out. In the followings we describe one experiment in details. A dedicated experiment was conducted in a controlled environment at the PTB antenna test facility in Braunschweig, i.e. an environment where only one ground reflection would occur (Figure 5). Two antennas were set up with different heights above the reflector. The antennas were spaced about 21.3 m. The observation period lasted for about 7 hours and a cut-off angle of 0° was applied. The data rate was 1 Hz. One pair of AX1202GG LEICA antennas were used together with LEICA GRX1200+GNSS receivers.

http://dx.doi.org/10.5772/54567

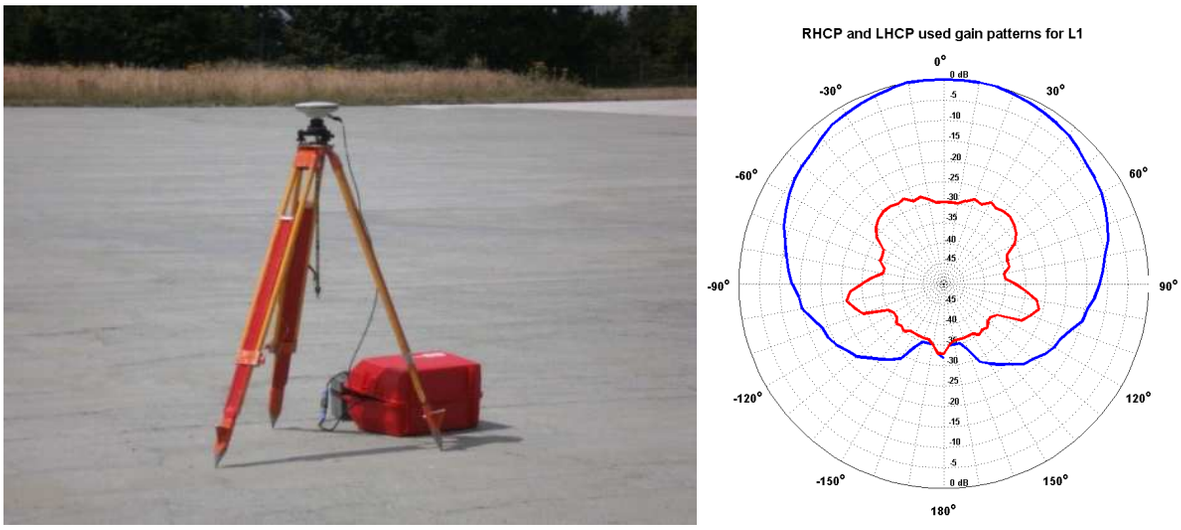

Figure 5. Left: Experimental set up of the Leica AX1202GG antenna. Right: The NOV702GG gain patterns [dB] for both orthogonal polarizations (RHCP in blue and LHCP in red) were used to model the antenna. Adopted from [77]

4.2. Simulations

The following assumptions were used for the simulations: The receiving antenna gain patterns are taken from a NOV702GG antenna assumed to be similar to the AX1202 (see Figure 5). The normalized gain patterns were assumed symmetrical in azimuth. In this way the Jones vector of the receiving antenna for all possible azimuths and elevation angles of the incoming LOS and MPCs GNSS signals can be computed as in eq. (21). The satellite antenna was assumed here perfect RHCP and modeled as:

$$\vec{e}_{trans} = \frac{1}{\sqrt{2}}\begin{bmatrix}1\\ -j\end{bmatrix} \tag{33}$$

Finally, for simplicity the angles ψ_{rec} and ψ_{trans} were assumed to be equal and constant over time. Absolute and individual antennas phase center corrections from IfE Hannover were also taken into account during data processing. Furthermore, it is assumed that the ground reflector is a perfect horizontal reflector. Using eq. (27) and (29), the simulated time series for the phase error and the compound signal amplitude (dB) were computed. Under the assumption the values are independent of the satellite azimuth; one exemplary satellite (PRN 12) is plotted covering the whole elevation range. Two different antenna heights above the reflector were used according to the measuring set up. The heights of the two antennas A1, A2 were 1.358 m and 2.053 m, respectively.

In Figure 6, simulated normalized amplitudes [dB] of the MPC, the direct and compound signals are plotted for PRN12 versus satellite elevation for both antennas of the observed baseline. The direct signal's amplitude is plotted in red, the amplitude of the compound signal

in blue, and in black the difference between the direct signal and the compound one is given, thus the impact of the multipath.

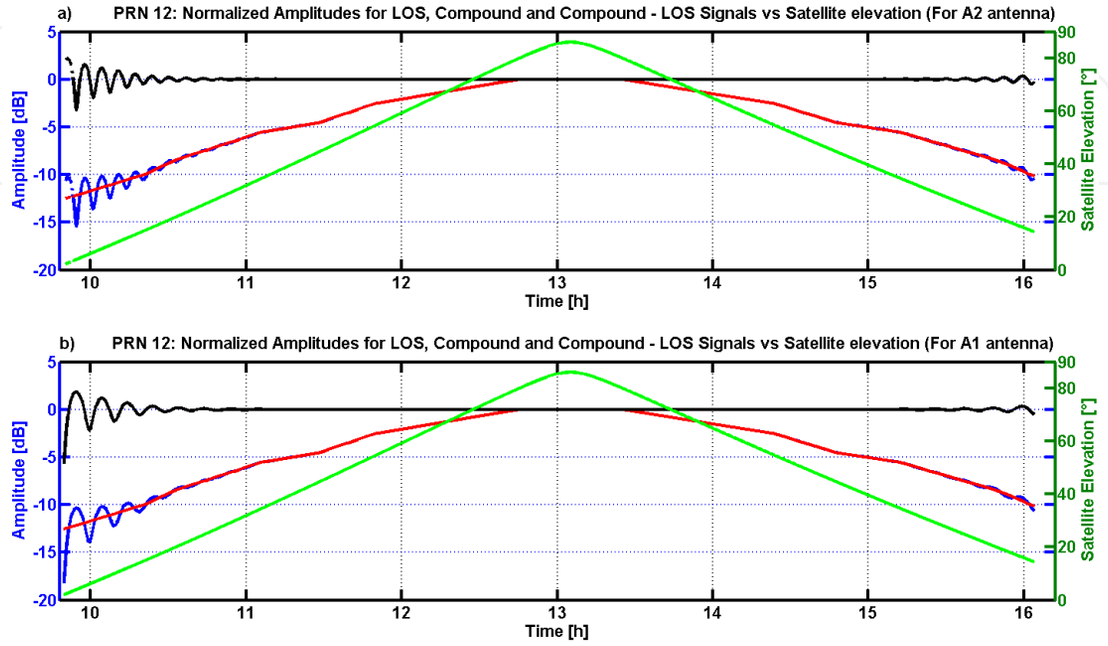

Figure 6. Simulated and normalized amplitude values versus satellite elevation for PRN 12 and reflector made of concrete. a) LOS, ground MPC and compound signal amplitudes for antenna position A2. b) LOS, ground MPC and compound signal amplitudes for the antenna position A1.

The normalized amplitude of the LOS is a smooth curve mainly determined by the gain pattern of the receiving antenna. The resulting multipath effect (black) shows the typical amplitude variations of few dB. Finally, the compound amplitude shows a superposition of both features. Furthermore, a frequency difference of the oscillations can be noticed between the antennas, depending on the height difference. For the maximum elevation angle of 90° PRN 12 has a minimum attenuation of 0 dB. For the same satellite elevation, the amplitude of the ground MPC is almost -32 dB. The reason is that the reflected MPC, at a reflection angle of about 90° and with angle of arrival near -90° with respect to the antenna horizon, is almost LHCP (see Figure 3a) and it is strongly attenuated due to the LHCP gain pattern of the antenna for such angles of arrival (see Figure 5, right side). Thus, the LOS signal is dominating. At elevation angles near 0°, the MPC is still having most of the signal energy in the RHCP component (see Figure 3) and only a small part of it in the LHCP component. The relative amplitude α of the MPC w.r.t. LOS is about 0.6. So in this case, the MPC reflection loss is minimum, the MPC RHCP component is dominating and the antenna applies a very similar gain for both LOS and ground MPC signal components.

In a next step, the impact of different reflector material properties will be investigated. We chose exemplary material properties of perfect, concrete, sea water and wet ground reflectors (see Table 2). Since the impact will be much stronger at low elevation angles, only a part of the

http://dx.doi.org/10.5772/54567

arc of PRN 12 is plotted. Figure 7 shows the resulting curves for the compound signal amplitude for two different antenna heights.

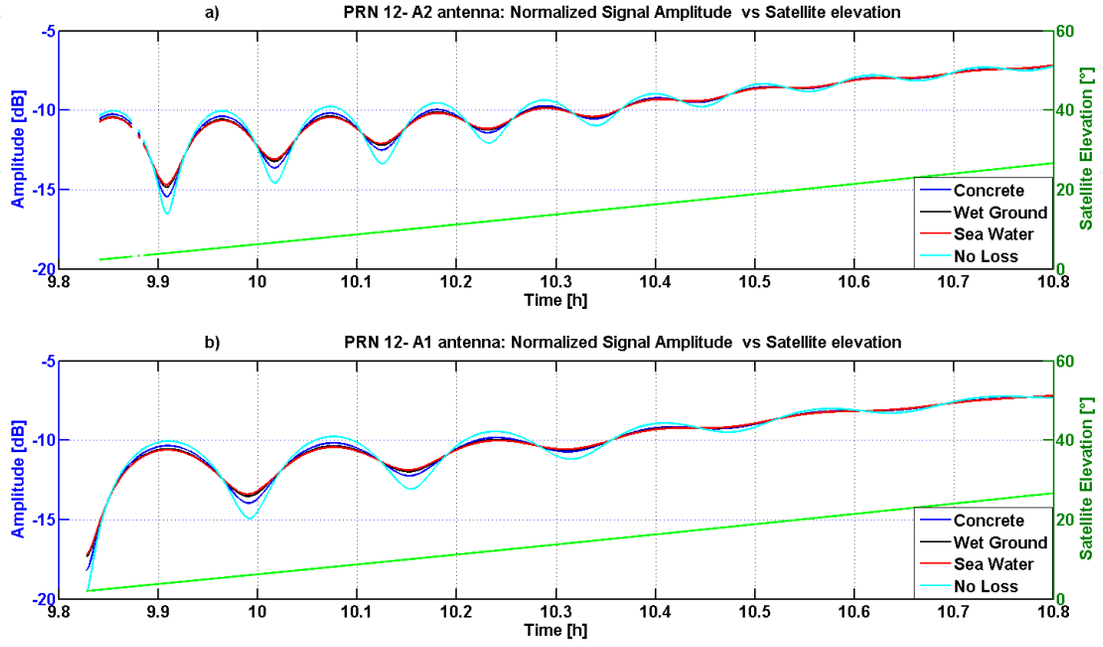

Figure 7. Normalized amplitude in [dB] of the compound signal for different material properties. Zoom at low elevation angles. (a): antenna A2, 2.053 m above the reflector, (b): antenna A1, 1.358 m above the reflector.

The change in the material properties creates mainly a change in the amplitude of the variations. A perfect reflector creates the strongest oscillation. The concrete reflector is also creating MPC with higher amplitude than water reflector and the wet ground reflector. This is because for small reflection angles the material properties of concrete are causing a smoother change of the signal polarizations (from RH to LH) in contrast to the reflections coefficients of the other two reflectors that are creating a more abrupt change (see Figures 3).

4.3. Comparison of simulations and real data

The C/N_0 values obtained from the RINEX observation files can be compared with the simulated values. In Figure 8 for two exemplary satellites, PRN 12 and PRN 14, the corresponding time series are compared. Here, only the data for the antenna A1 at a height of 1.358 m above the reflector is considered. The reflection properties are modeled for a concrete reflector (see Table 2). Both curves show that the simulations can explain the main features present in the observations. The scale on both axes is the same. However, some disturbances occur which are due to our simplifications, e.g. neglecting a small tilting of the reflector, the approximated satellite and receiver antenna patterns.

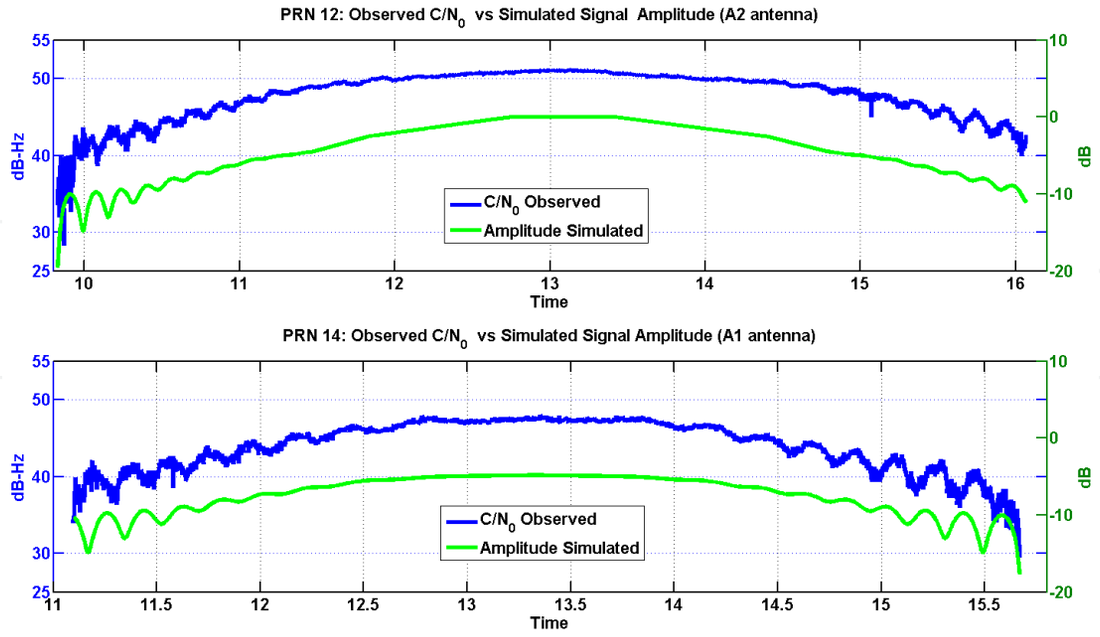

Figure 8. Observed C/N_0 values versus simulated signal amplitude for PRN 12 and 14 for antenna A1

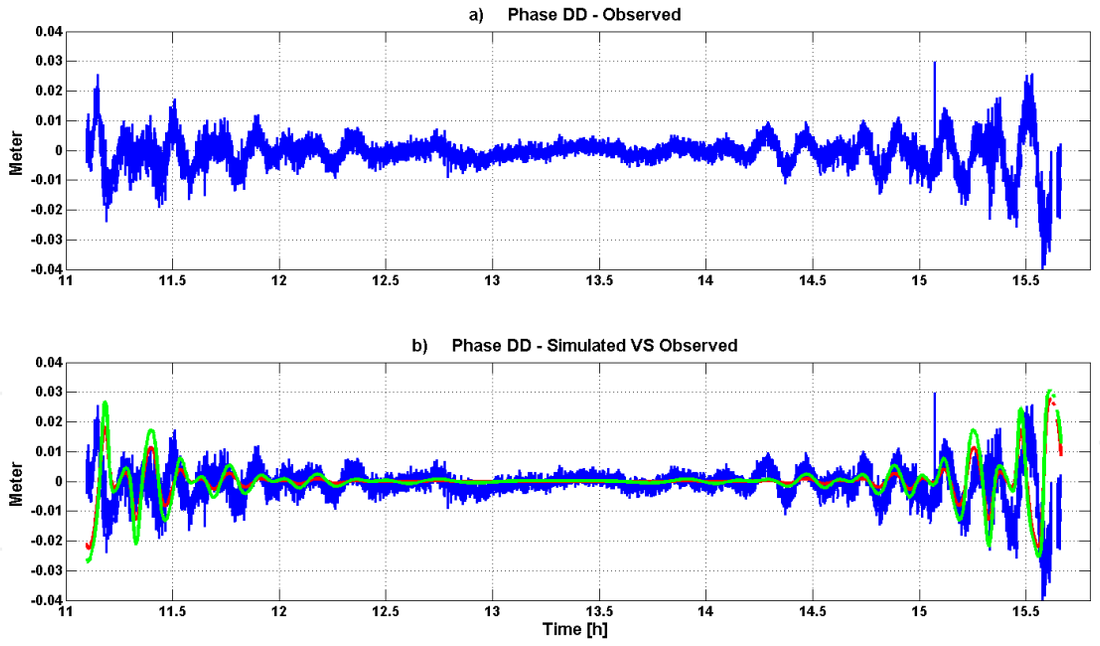

Figure 9. Simulated phase error - DD values versus observed phase DD (in blue) formed from PRN 12 and 14. Simulated DD for a concrete reflector are indicated in red and for a perfect reflector in green.

Finally, the carrier phase observations are investigated. To this end, double-differences (DD) are formed between the two antennas on the short baseline. Thus, most distance-dependent systematics as well as the receiver clock errors will cancel out. Again we use PRN 12 and 14. In Figure 9, the phase DD formed by PRN 12 and 14 of the short baseline are plotted together

with double-differenced simulated phase error as in eq. (27). The time series of the observed values for an observational period of about 4.5 hours are plotted in blue in Figure 9a). In Figure 9b) the time series is overlaid by the simulated DD phase errors, where the relative amplitude of each multipath component is calculated analytical. In green no reflection loss is considered and in red the material properties of a concrete reflector are used.

5. Conclusion

Multipath propagation is still limiting the accuracy of precise GNSS applications despite the four decades of intensive research in this field. Signal amplitude, both for direct and indirect GNSS signal components that arrive at the receiving antenna with small relative delays, are crucial for the resulting phase error magnitude due to multipath propagation.

After a short introduction and a discussion on the different approaches that can be found in literature, aspects of ray propagation and signal polarization modeling are introduced. Then, an extensive description of the reflection process and its impact on the polarization state of the reflected signals is presented and all involved parameters are characterized. An analytical model for GNSS signal amplitudes is presented after. The model is then integrated into the equations for the phase error and the compound signal amplitude. Simulated and real data from a dedicated experiment are used to highlight the main properties of multipath propagation on the signal amplitude and carrier-phase domains.

Acknowledgements

This work has been realized within the BERTA project (50NA1012), funded by the Federal Ministry of Economics and Technology, and based on a resolution by the German Bundestag. The authors thank the BERTA partner Prof. Thomas Kürner (Institut für Nachrichtentechnik, TU Braunschweig) for the fruitful discussions. The authors would like to thank Dr. Thorsten Schrader (PTB Braunschweig) for supporting the experiments at the antenna reference open area test site at PTB.

Author details

Marios Smyrnaios[1*], Steffen Schön[1] and Marcos Liso Nicolás[2]

*Address all correspondence to: smyrnaios@ife.uni-hannover.de

1 Institut für Erdmessung, Leibniz-Universität Hannover, Hannover, Germany

2 Institut für Nachrichtentechnik Technische Universität Braunschweig, Braunschweig, Germany

References

[1] L. Hagerman, Effects on multipath of coherent and non coherent PRN ranging receiver, The Aerospace Corporation, 1973.

[2] Y. Georgiadou and A. Kleusberg, On carrier signal multipath effects in relative GPS positioning, *Manuscripta Geodaetica, 13,* pp. 172-179, 1988.

[3] M. Braasch, Multipath effects, in *GPS Positioning System Theory and Applications Vol. 1*, vol. Progress in Astronautics and Aeronautics Vol. 163., 1996, pp. 547-568.

[4] G. Seeber, Satellite Geodesy, Walter de Gruyter, 2003 2nd edition, pp. 316 - 320.

[5] A. Leick, GPS Satellite Surveying, Hoboken, New Jersey: John Wiley & Sons, Inc., 2004, pp. 237 - 243.

[6] B. Hofmann-Wellenhof, H. Lichtenegger and E. Wasle, GNSS Global Navigation Satellite Systems, Springer Wien New York, 2008, pp. 154 - 160.

[7] B. Hannah, Modeling and Simulation of GPS Multipath Propagation, Queensland: Queensland University of Technology, 2001, PhD thesis.

[8] L. Lau, Phase Multipath Modeling and Mitigation in Multiple Frequency GPS and Galileo Positioning, London: University College London, University of London, 2005, PhD thesis.

[9] M. Irsigler, Multipath propagation, mitigation and monitoring in the light of Galileo and the modernized GPS, München, 2008, PhD thesis.

[10] C. Rost, Phasenmehrwegereduzierung basierend auf Signalqualitätsmessungen geodätischer GNSS-Empfänger, Bayerische Akademie der Wissenschaften, 2011, Nr 665, PhD thesis.

[11] R. Van Nee, Multipath and Multi-Transmitter Interference in Spread-Spectrum Communication and Navigation Systems, Delf: Delf University of Technology, 1995, PhD thesis.

[12] J. Ray, Mitigation of GPS Code and Carrier Phase Multipath Effects Using a Multi-Antenna System, University of Calgary, Calgary, Alberta, Canada, 2000, PhD thesis.

[13] A. Bilich , Improving the Precision and Accuracy of Geodetic GPS: Application to Multipath and Seismology, Colorado: University of Colorado, 2006, PhD thesis.

[14] J. Weiss, Modeling and Characterization of Multipath in Global Navigation Satellite System Ranging Signals, Colorado: University of Colorado, 2007, PhD thesis.

[15] V. Böder, Zur hochpräzisen GPS-Positions- und Lagebestimmung unter besonderer Berücksichtigung mariner Anwendungen, Hannover: Wissenschaftliche Arbeiten der Fachrichtung Geodäsie und Geoinformatik der Universität Hannover, Nr. 245, 2002, PhD thesis.

[16] F. Dilssner, Zum Einfluss des Antennenumfeldes auf die hochpräzise GNSS-Positionsbestimmung, Hannover: Wissenschaftliche Arbeiten des Fachrichtung Geodäsie und Geoinformatik der Leibniz Universität Hannover, Nr. 253, 2008, PhD thesis.

[17] P. Misra and P. Enge, Global Positioning System: Signals, Measurements, and Performance, Jamuna Press, 2006, 2nd edition.

[18] R. Hatch , Dynamic advanced GPS at the centimeter level, in *Proceedings of the 4th international geodetic symposium on satellite positioning*, Austin, Texas, 1986.

[19] R. van Nee , Multipath effects on GPS code phase measurements, in *Proceedings of the 4th International Technical Meeting of the Satellite Division of The Institute of Navigation (ION GPS 1991)*, Washington, DC, September 11 - 13, 1991.

[20] C. Rocken, C. Meertens, B. Stephens, J. Braun, T. Van Hove, S. Perry, O. Ruud, M. McCallum and J. Richardson, UNAVCO Academic Reaserch Infrastructure (ARI) Receiver and Antenna Test Report, 1996.

[21] L. Wanninger and M. May, Carrier Phase Multipath Calibration of GPS Reference Stations, in *Proceedings of the 13th International Technical Meeting of the Satellite Division of The Institute of Navigation (ION GPS 2000)*, Salt Lake City, Utah, September 19 - 22, 2000.

[22] J. Genrich and Y. Bock , Rapid resolution of crustal motion at short ranges with the global positioning system., in *Geophys Res Lett 97:3261-3269*, 1992.

[23] D. Agnew and K. Larson, Finding the repeat times of the GPS constallation., *GPS Solution,* vol. 11, pp. 71-76, 2007.

[24] F. Dilssner, G. Seeber, G. Wübbena and M. Schmitz, Impact of Near-Field Effects on the GNSS Position Solution, in *Proceedings of the 21st International Technical Meeting of the Satellite Division of The Institute of Navigation (ION GNSS 2008), pp. 612-624* , Savannah, GA , September 16 - 19, 2008.

[25] C. Granström and J. Johansson , Site-Dependent Effects in Hight-Accuracy Applications of GNSS, In Report on the Symposium of the IAG Subcommission for Europe (EUREF)., London, 2007.

[26] T. Iwabuchi, Y. Shoji, S. Shimada and H. Nakamura, Tsukuba GPS Dense Net Campaign Observations: Comparison of the Stacking Maps of Post-fit Phase Residuals Estimated from Three Software Packages, *Journal of the Meteorological Society,* vol. 82(1B), pp. 315-330, 2004.

[27] C. Rost and L. Wanninger, Carrier phase multipath mitigation based on GNSS signal quality measurements, *Journal of Applied Geodesy, 3(2), 81- 87.103,* 2009.

[28] P. Axelrad, C. Comp and P. Macdoran , SNR-based multipath error corection for GPS differential phase., in *IEEE Transaction on Aerospace and Electronic Systems*, 1996, 32(2), 650-660.99.

[29] A. Bilich , K. Larson and P. Axelrad, Modeling GPS phase multipath with SNR: Case study from the Salar de Uyuni, Boliva, *Journal of Geophysical Research,* vol. 113, 2008.

[30] Leica, http://www.surveyequipment.com/PDFs/AR25_Brochure.pdf, Leica AR25. [Online].

[31] L. Lau and P. Cross, A new signal-to-noise-ratio based stochastic model for GNSS highprecision carrier phase data processing algorithms in the presence of multipath errors, in *Proceedings of the 19th International Technical Meeting of the Satellite Division of The Institute of Navigation (ION GNSS 2006)*, Fort Worth, Texas, September 26 - 29, 2006.

[32] H. Hartinger and F. Brunner, Variances of GPS phase observations: the SIGMA-ε model, *GPS Solutions,* pp. Volume 2, Issue 4 , pp 35-43, 1999.

[33] A. Wieser, Robust and fuzzy techniques for parameter estimation and quality assessment in GPS, Graz, Technische Universität Graz, 2001, PhD thesis.

[34] A. Van Dierendonck, P. Fenton and T. Ford, Theory and performance of narrow correlator spacing in a GPS receiver, *Journal of the Institute of Navigation,* Vols. 39(3), 265-283.47, 90, 1992.

[35] G. McGraw and M. Braasch, GNSS multipath mitigation using Gated and High-Resolution correlator concepts, in *Proceedings of the 1999 National Technical Meeting of The Institute of Navigation*, San Diego, California, January 25 - 27, 1999, 333-342.

[36] L. Garin, F. van Diggelen and J. Rousseau, Storbe and Edge Correlator multipath mitigation for code, in *Proceedings of the 9th International Technical Meeting of the Satellite Division of The Institute of Navigation (ION GPS 1996)*, Kansas City, Missouri, September 17 - 20, 1996, 657-664.

[37] L. Garin and J. Rousseau, Enhanced Storbe Correlator Multipath Rejection for Code and Carrier, in *Proceedings of the 10th International Technical Meeting of the Satellite Division of The Institute of Navigation (ION GPS 1997)*, Kansas City, Missouri, September 16 - 19, 1997, 559-568.

[38] P. Fenton and J. Jones, Theory and Performance of Novatel Inc.'s Vision Correlator, in *Proceedings of the 18th International Technical Meeting of the Satellite Division of The Institute of Navigation (ION GNSS 2005)*, Long Beach, California, September 13 - 16, 2005, 2178 - 2186.

[39] B. Townsend, R. Van Nee, P. Fenton and K. Van Dierendonck, Performance Evaluation of the Multipath Estimating Delay Lock Loop, *Navigation,* Vols. 42, No. 3, pp. 503-514, 1995.

[40] B. Townsend , P. Fenton , K. Van Dierendonck and R. Van Nee, L1 Carrier Phase Multipath Error Reduction Using MEDLL Technology, in *Proceedings of the 8th International Technical Meeting of the Satellite Division of the Institute of Navigation, ION - GPS 1995*, Palm Springs, California, 1995, 1539-1544.

[41] R. Lawrence, How Good Can It Get with New Signals? Multipath Mitigation, *GPS World*, 2003.

[42] A. Van Dierendonck, Evaluation of GNSS Receiver Correlation Processing Techniques for Multipath and Noise Mitigation, in *Proceedings of the 1997 National Technical Meeting of The Institute of Navigation*, Santa Monica, CA, January 14 - 16, 1997, 207-215.

[43] K. Borre, D. Akos, N. Bertelsen, P. Rinder and S. Jensen, A Software-Defined GPS and Galileo Receiver. A Single Frequency Approach, Boston: Birkhäuser, 2007.

[44] J. Tsui, Fundamentals of Global Positioning System Receivers. A Software Approach, New York: John Wiley & Sons, INC, 2000.

[45] T. Pany, Navigation Signal Processing for GNSS Software Receivers, Artech House, 2010.

[46] G. Moernaut and D. Orban, GNSS Antennas An Introduction to Bandwidth, Gain Pattern, Polarization, and All That, *GPS World*, pp. 42 - 48, February 2009.

[47] J. Tranquilla, J. Carr and H. Al-Rizzo, Analysis of a choke ring groundplane for multipath control in Global Positioning Systems (GPS) applications, in *IEEE Transactions on Antennas and Propagation, 42(7), 905-911*, 1994.

[48] T. Blakney, D. Connell, B. Lamberty and J. Lee, Broad-band antenna sructure having frequency-independent, low loss ground plane (Patent Nr. 4608572), Seattle, WA, 1986.

[49] V. Filippov, I. Sutiadin and J. Ashjaee, Measured Characteristics of Dual Depth Dual Frequency Choke Ring for Multipath Rejection in GPS Receivers, in *In Proceedings of the 12th International Technical Meeting of the Satellite Division of the Institute of Navigation (ION GPS 1999), 793 – 796*, Nashville, 1999.

[50] T. Ning, G. Elgered and J. Johansson, The impact of microwave absorber and radome geometries on GNSS measurements of station coordinates and atmospheric water vapour, *Adv Space Sci, 47(2), 186*, 2011.

[51] J. Ray, M. Cannon and P. Fenton , Mitigation of Static Carrier Phase Multipath Effects Using Multiple Closely-Spaced Antennas, in *Proceedings of the 1th International Technical Meeting of the Satellite Division of the Institute of Navigation, ION - GPS98*, Nashville, Tennessee, September 15-18, 1998, 1025-1034.

[52] M. Cuntz, H. Denks, A. Konovaltsev, A. Hornbostel, A. Dreher and M. Meurer, GALANT - Architecture Design and First Results of A Novel Galileo Navigation Receiver Demonstrator With Array Antennas, in *Proceedings of the 21st International Technical Meeting of the Satellite Division of the Institute of Navigation* , Savannah, september 16-19, 2008, pp. 1470-1476.

[53] K. Park, P. Elosegui, J. Davis, P. Jarlemark, B. Corey, A. Niell, J. Normandeau, C. Meertens and V. Andreatta, Development of an Antenna and Multipath Calibration System for Global Positioning System Sites, *RADIO SCIENCE*, vol. 39, 2004.

[54] V. Böder , F. Menge , G. Seeber, G. Wübbena and M. Schmitz, How to Deal With Station Dependent Errors - New Developments of Absolute Field Calibration of PCV and Phase-Multipath With a Precise Robot, in *ION 2001*, Salt Lake City, Utah, 2001.

[55] G. Wübbena, M. Schmitz and G. Boettcher, Near-field Effects on GNSS Sites: Analysis using Absolute Robot Calibration and Procedures to Determine Corrections, in *IGS Workshop* , Drmstadt, Germany, 2006.

[56] P. Shetty, A. Kakkar, U. Weinbach and S. Schön, Experimental Analysis of Multipath Linear Combination of GPS and Galileo Signals, Poster, in *Geodätische Woche*, Köln, Oktober 5-7, 2010.

[57] E. Schönemann , A. Hauschild, P. Steigenberger, T. Springer, J. Dow, O. Montenbruck, U. Hugentobler and M. Becker, New Results from GIOVE: The CONGO-Network and the Potential of Tracking Networks with Multiple Receiver and Antenna Types, in *EGU General Assembly*, Vienna, Austria, 2010.

[58] O. Montenbruck, A. Hauschild and U. Hessels, Characterization of GPS/GIOVE Sensor Stations in CONGO Network, *GPS Solution, 15(3), 193-205,* 2011.

[59] P. Elósegui, J. Davis, R. Jaldehag, J. Johansson, A. Niell and I. Shapiro, Geodesy using the Global Positioning System: The effects of signal scattering on estimates of site position, *Journal of Geophysical Research, 100(B7), 9921-9934,* 1995.

[60] M. Liso , M. Smyrnaios, S. Schön and T. Kürner, Basic Concepts for the Modeling and Correction of GNSS Multipath Effects Using Ray-Tracing and Software Receivers, in *IEEE APS Topical Conference on Antennas and Propagation in Wireless Communication*, Torino, Italy, 2011.

[61] J. Bradbury, M. Ziebart, P. Cross, P. Boulton and A. Read, Code multipath modelling in the urban environment using large virtual reality city models: Determining the local environment, *Journal of Navigation, 60(1), 95-105,* 2007.

[62] A. Steingass and A. Lehner, Measuring the Navigation Multipath Channel … A Statistical Analysis, *Proceedings of the 17th International Technical Meeting of the Satellite Division of The Institute of Navigation (ION GNSS 2004)*, September 21 - 24, 2004, pp. 1157 - 1164.

[63] R. Treuhaft, S. Lowe, C. Zuffada and Y. Chao, 2-cm GPS altimetry over Crater Lake, *Geophysical Research Letters, 22(23), 4343-4346,* 2001.

[64] A. Helm, Ground-based GPS Altimetry with the L1 Open GPS receiver using carrier phase-delay observations of reflected GPS signals, Scientific Technical report STR08/10,GFZ Potsdam, Potsdam, 2008, PhD thesis.

[65] J. Garrison, S. Katzberg and C. Howell, Detection of Ocean Reflected GPS Signals: Theory and Experiment, in *Proceedings of the IEEE Southeast*, Blacksburg, USA, April 12-14, 1997, pp. 290-294.

[66] K. Larson, E. Small, E. Gutmann, A. Bilich, P. Axelrad and J. Braun, Using GPS multipath to measure soil moisture fluctuations: initial results, *GPS Solution, Vol 12(3),* pp. 173-177, 2008.

[67] M. Martin-Neira, A Passive Reflectometry and Interferometry System (PARIS): Application to Ocean Altimetry, *ESA Journal,* vol. 17(4), pp. 331-355, 1993.

[68] V. Zavorotny, K. Larson, J. Braun, E. Small, E. Gutmann and A. Bilich, A physical model of GPS multipath caused by land reflections: toward bare soil moisture retrievals, in *IEEE J-STARS*, 2010.

[69] A. Rius, J. Aparicio, E. Cardellach and M. Martin-Neira, Sea Surface State Measured Using GPS Reflected Signals, *Geophysical Reaserch Letters,* vol. 29(23), 2002.

[70] W. Stutzman, Polarization in Electromagnetic Systems, Artech House, Boston - London, 1993.

[71] C. Balanis, Antenna Theory, New Jersey: John Wiley & Sons, Inc., 2005.

[72] J. Peatross and M. Ware, Physics of Light and Optics, Brigham Young University, 2008.

[73] A. Maltsev, V. Erceg, E. Perahia, C. Hansen, R. Maslennikov, A. Lomayev, A. Sevastyanov and A. Khoryaev, Polarization model for 60 GHz WLAN Systems, 2009.

[74] A. Maltsev, R. Maslennikov, A. Lomayev, A. Sevastyanov and A. Khoryaev, Statistical Channel Model for 60 GHz WLAN Systems in Conference Room Enviroment, *Radioengineering,* vol. 20, pp. 409-422, June 2011.

[75] W. Marquis and D. Reigh, On-Orbit Performance of the Improved GPS Block IIR Antenna Panel, in *Proceedings of the 18th International Technical Meeting of the Satellite Division of The Institute of Navigation (ION GNSS 2005)*, Long Beach, CA, September 13 - 16, 2005.

[76] "ICD-GPS-200c 10-10-1993 to 12-4-2000".

[77] "GPS-701-GG and GPS-702-GG Antennas," Novatel, [Online]. Available: http://webone.novatel.ca/assets/Documents/Papers/GPS701_702GG.pdf.

[78] F. Czopek and S. Shollenberger, Description and Performance of the GPS Block I and II L-Band Antenna and Link Budget, in *Proceedings of the 6th International Technical Meeting of the Satellite Division of The Institute of Navigation (ION GPS 1993)*, Salt Lake City, UT, 37-43, September 22 - 24, 1993.

[79] S. Ericson, K. Shallberg and C. Edgar, Characterization and Simulation of SVN49 (PRN01) Elevation Dependent Measurement Biases, in *Proceedings of the 2010 International Technical Meeting of The Institute of Navigation*, San Diego, CA, January 25 - 27, 2010.

IntechOpen